Patch diameter limits for tiered subaperture SAR image formation algorithms

Armin Doerry

Sandia National Laboratories
PO Box 5800, MS 0529, Albuquerque, NM, 87185-0529

ABSTRACT

Synthetic Aperture Radar image formation algorithms typically use transform techniques that often requires trading between image resolution, algorithm efficiency, and focussed image scene size limits. This is due to assumptions for the data such as simplified (often straight-line) flight paths, simplified imaging geometry, and simplified models for phase functions. Many errors in such assumptions are typically untreatable due to their dependance on both data domain positions and image domain positions. The result is that large scenes often require inefficient multiple image formation iterations, followed by a mosaicking operation of the focussed image patches. One class of image formation algorithms that performs favorably divides the spatial and frequency apertures into subapertures, and perhaps those subapertures into sub-subapertures, and so on, in a tiered subaperture fashion. This allows a gradual shift from data domain into image domain that allows correcting many types of errors that limit other image formation algorithms, even in a dynamic motion environment, thereby allowing larger focussed image patches without mosaicking. This paper presents and compares focussed patch diameter limits for tiered subaperture (TSA) image formation algorithms, for various numbers of tiers of subapertures. Examples are given that show orders-of-magnitude improvement in non-mosaicked focussed image patch size over traditional polar format processing, and that patch size limits increase with the number of tiers of subapertures, although with diminishing returns.

Keywords: Synthetic Aperture Radar, SAR, Subaperture, Algorithm, Imaging, Limits, Phase Errors, Migration

1. INTRODUCTION

Synthetic Aperture Radar (SAR) is used to form images of radar reflectivity over some scene of interest. The precision with which a reflectivity value can be assigned to a location is the resolution. SARs form an image from range soundings taken from discrete points in the space around the scene. This collection of spatial points is the synthetic aperture, and larger synthetic apertures are required for finer resolutions. The variation in range from each of the many spatial sample points to a particular scene location is unique from any other scene location, and, when measured by the phase of the radar return, is the doppler signature. This uniqueness allows the matched filtering of the spatial sample data to localize that scene's reflectivity, but each location in the scene optimally requires its own matched filter, making matched filtering prohibitively expensive. Realizing that the range function doesn't behave too differently for a neighborhood around some focal point, and the differences exhibit strong linear relationships with scene location, allows the use of transform techniques such as the Discrete Fourier Transform (DFT), or its fast implementation, the Fast Fourier Transform (FFT), to form an image with considerable improvement in computational efficiency. However, for large neighborhoods of scene locations, the linear relationships break down, making processing with a single transform less and less suitable as distance from the central reference point, or focal point, increases. The data exhibits 'migration errors' and 'spatially variant phase errors' which degrade image quality, ultimately beyond some tolerable threshold, which sets the scene size limit. This limit is less for finer resolution, and particularly troublesome as resolution approaches the nominal wavelength of the radar. The challenge becomes to mitigate the migration errors and spatially variant phase errors, and form images of large scenes at fine resolution using efficient transform techniques.

A number of algorithms have been developed to form fine resolution images of large scenes.[1] One of the most recent is 'wave-number domain', or 'migration' processing, which operates in the frequency domain. This technique requires a linear flight path and doesn't tolerate flight path deviations (especially out-of-plane motion) very well.[6] Two fairly successful image formation algorithms for airborne SARs are 'Polar Format' processing, and 'Overlapped Subaperture' (OSA) processing,[2,9] which both operate to some degree in the azimuth time domain, making them capable of dealing fairly effectively with flight path deviations. However, both algorithms still have scene size limits that are especially severe as resolutions approach a wavelength, such as is desired at UHF and lower frequencies. Large scenes require multiple image formation operations

followed by a mosaicking of patches of finished subimages. Efficiency is lost when mosaicking requires too many subimages. This has led to the proposal of using multiple levels of tiered subapertures to form ever finer resolution intermediate images, and allow error corrections along the way, as an image formation strategy that can be scaled to much larger scene sizes than are currently achievable.[4,5,8]

This paper introduces and summarizes the analysis of generalized 'Tiered Subaperture' (TSA) techniques that are a superset of both Polar Format processing and OSA processing. It is shown how tiers of subapertures in both azimuth and range can effectively mitigate both migration errors and spatially variant phase errors to allow virtually arbitrary scene sizes, even in a dynamic motion environment. This paper presumes a spotlight mode SAR with a linear-frequency-modulated (LFM) chirp that is deramped upon reception (stretch-processing[3]). These concepts are clarified in the appropriate sections.

2. ONE DIMENSIONAL ANALOGY

Consider a function of the form

$$f(n) = \exp j\left(\omega n + a\omega^2 n^2\right), \qquad -\pi \le -\Omega/2 \le \omega \le \Omega/2 < \pi \qquad N/2 \le n \le N/2 - 1 \qquad (1)$$

with known constant a, $0 < a \ll 1$. The challenge is to determine ω with acceptable precision and accuracy within the range $|\omega| \le \Omega/2$, and efficiently.

If a were zero, the task would simply amount to a DFT across n. This locates ω with resolution of about $2\pi/N$, depending on window functions employed, and how specifically resolution is measured. For this case, larger N means finer resolution, without bound.

For nonzero a, we must consider the quadratic phase term (quadratic in n). For small enough Ω and/or small enough N, this term is sufficiently small, say $\le \pi/2$, and can be ignored. A reasonable criteria might then be

$$\Omega \le \rho\sqrt{2/(\pi a)} \quad , \qquad (2)$$

where $\rho = 2\pi/N$ is the nominal resolution of the DFT.

As an example, consider a signal that is the linear sum of four separate component signals, each of which can be expressed by equation (1), but with individual ω from the set $\{0, \pi/4, \pi/2, 3\pi/4\}$. For all component signals, let $N = 256$ and $a = 0.0001$. Figure 1 illustrates the DFT of the total signal. Clearly, resolution is lost as ω is increased.

Here we see the basic dilemma. By using the DFT, the finer the resolution ρ with which we wish to identify ω, the smaller the range Ω is over which we can acceptably resolve ω. In SAR processing, the analogs are that frequency ω corresponds to target distance from the scene center, or focal point. The frequency range Ω corresponds to scene diameter, and frequency resolution corresponds to SAR spatial target resolution. For our analog, the challenge becomes to exceed the limit in equation (2). To do this we need to mitigate the effects of the quadratic phase term in equation (1), which is an error term that limits DFT processing.

2.1. Subapertures

We do this by making a coarse resolution estimate of ω, and use this to compensate $f(n)$ before proceeding with a fine resolution estimate. Conceptually, we make coarse resolution estimates of ω by dividing the aperture into subapertures, as is illustrated in figure 3. Mathematically, we do this by splitting the domain of index n into groups of indices m_1 and m_2, as follows,

$$n = m_1 + \Delta_2 m_2 \quad , \qquad -M_1/2 \le m_1 \le M_1/2 - 1 \, , \qquad -M_2/2 \le m_2 \le M_2/2 - 1 \, , \qquad (3)$$

where Δ_2 is a data decimation factor, with subapertures overlapped by an amount $(M_1 - \Delta_2)$. Overlapping subapertures is necessary to control sidelobes. Function *f(n)* can be expanded to

$$f(n) = f(m_1, m_2) = \exp j\left(\omega\Delta_2 m_2 + a\omega^2\Delta_2^2 m_2^2\right)\exp j\left(\left(\omega + 2a\omega^2\Delta_2 m_2\right)m_1 + a\omega^2 m_1^2\right). \quad (4)$$

The strategy becomes to perform a DFT across index m_1, and do this for each index value m_2, which will yield a coarse resolution estimate of ω,

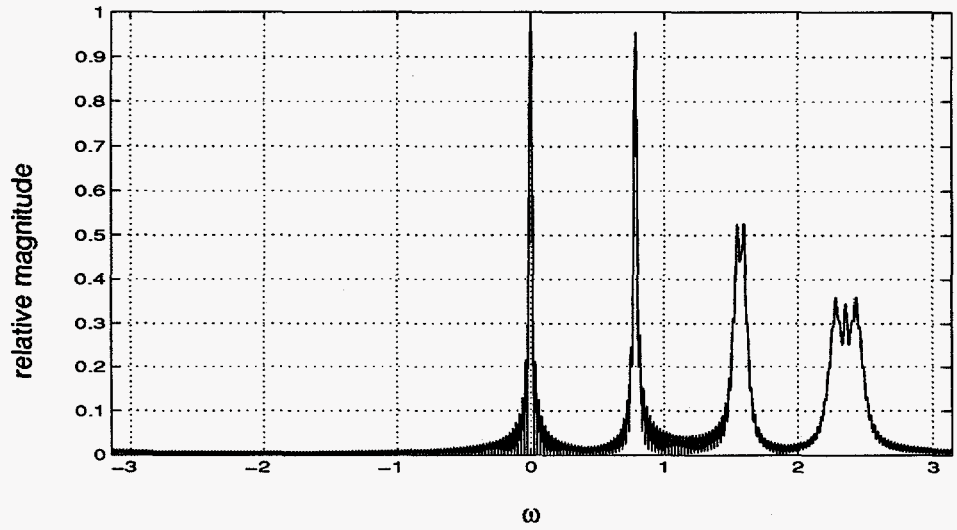

Figure 1. DFT of signals with quadratic phase errors.

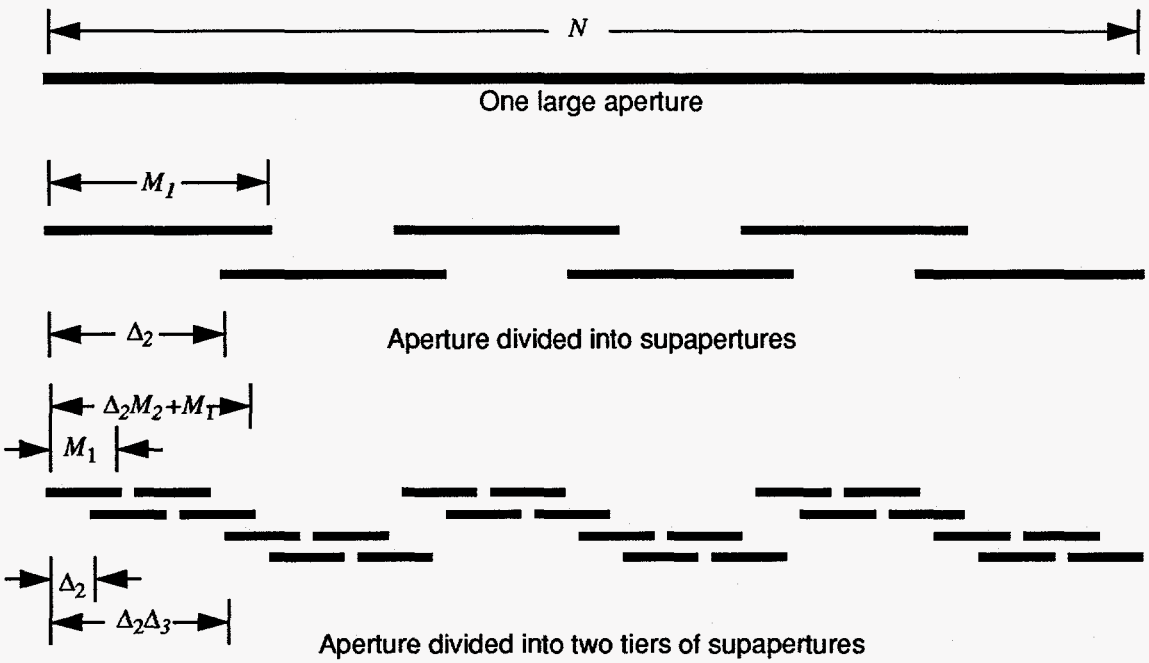

Figure 2. Aperture divided into subapertures.

$$\hat{\omega}_1 = \hat{\omega}(u_1) \approx \frac{2\pi u_1}{M_1} - 2a\hat{\omega}_1^2 \Delta_2 m_2, \qquad -M_1/2 \le u_1 \le M_1/2 - 1. \tag{5}$$

Note how this estimate migrates with subaperture index value m_2. With large enough m_2, the migration will transcend several resolution cells (values of u_1). Therefor, for any one value of u_1, the migration has the effect of 'windowing' the data over index m_2, as the amplitude peak moves into, and then out of, the appropriate resolution cell u_1. Since we will ultimately want to perform a DFT across index m_2, and we wish not too much unnecessary windowing of the data, it is desirable for the migration to be no more than about one coarse resolution cell $\rho_1 = 2\pi/M_1$ in total, over all m_2 for any ω. The result of the first DFT can then be approximated with

$$f_1(u_1, m_2) \approx \text{csinc}_{M_1}\left[\frac{M_1}{2}\left(\omega - \frac{2\pi u_1}{M_1}\right)\right] \exp j\left(\omega \Delta_2 m_2 + a\omega^2 \Delta_2^2 m_2^2\right), \tag{6}$$

where $\text{csinc}_N(x) \equiv \dfrac{\sin(x)}{\sin(x/N)} e^{-j(x/N)}$.

The estimate of ω allows us to compensate, or 'focus', equation (6) prior to a DFT across m_2, in the manner

$$\begin{aligned} f_1^*(u_1, m_2) &= f_1(u_1, m_2) \exp j\left(-\hat{\omega}_1 \Delta_2 m_2 - a\hat{\omega}_1^2 \Delta_2^2 m_2^2\right) \\ &\approx \text{csinc}_{M_1}\left[\frac{M_1}{2}\left(\omega - \frac{2\pi u_1}{M_1}\right)\right] \exp j\left((\omega - \hat{\omega}_1)\Delta_2 m_2 + a\left(\omega^2 - \hat{\omega}_1^2\right)\Delta_2^2 m_2^2\right). \end{aligned} \tag{7}$$

The final DFT across m_2 yields the final, best estimate of ω as

$$\hat{\omega}_2 \approx \frac{2\pi u_1}{M_1} + \frac{2\pi u_2}{M_2 \Delta_2} = \frac{2\pi}{M_2 \Delta_2}\left(\frac{M_2 \Delta_2}{M_1} u_1 + u_2\right), \tag{8}$$

with a resolution of $\rho_2 = 2\pi/(\Delta_2 M_2)$.

Limiting migration to one resolution cell, and quadratic phase errors to $\pi/2$, allows an overall limit

$$\Omega \le \rho_2 \, 2^{-1/3} (\pi a)^{-2/3}, \tag{9}$$

which is larger than equation (2) by a factor $2^{-5/6}(\pi a)^{-1/6} \approx 0.4637 a^{-1/6}$.

Reconsider the earlier example of figure 1. Recall that $a = 0.0001$. Processing this example with M_1=16, M_2=32, and Δ_2=8, results in the estimates for ω in figure 3.

2.2. Multiple Tiers of Subapertures

The question becomes "if one level of subapertures is good, will more levels of subapertures be better?" The short answer is "yes". For N_s number of tiers of subapertures one can generalize the results as follows.

$$\Omega \le \rho_{(N_s+1)} \, 2^{\frac{-(2N_s-1)}{(N_s+2)}} (\pi a)^{\frac{-(N_s+1)}{(N_s+2)}}. \tag{10}$$

The improvement of each tier of subapertures is plotted in figure 4.

Zero-padding prior to each DFT, thereby oversampling the output of the k^{th} DFT by an independent factor a_{os,m_k}, further improves Ω to

$$\Omega \le \rho_{(N_s+1)} 2^{\frac{-(2N_s-1)}{(N_s+2)}} (\pi a)^{\frac{-(N_s+1)}{(N_s+2)}} \left[a_{os,m_{N_s}} a_{os,m_{(N_s-1)}} \ldots a_{os,m_1}\right]^{\frac{1}{(N_s+2)}}. \tag{11}$$

3. POLAR FORMAT SAR PROCESSING

Consider a linear-FM chirp radar, collecting echo samples along a flight path at positions indexed by n, $N/2 \le n \le N/2-1$, with geometry defined in figure 5. The echoes are deramped and sampled at relative times indexed by i, $I/2 \le i \le I/2-1$. The radar operates with center frequency ω_n, chirp rate γ_n, and ADC sample period T_s. The radar's sampled video signal can be described by

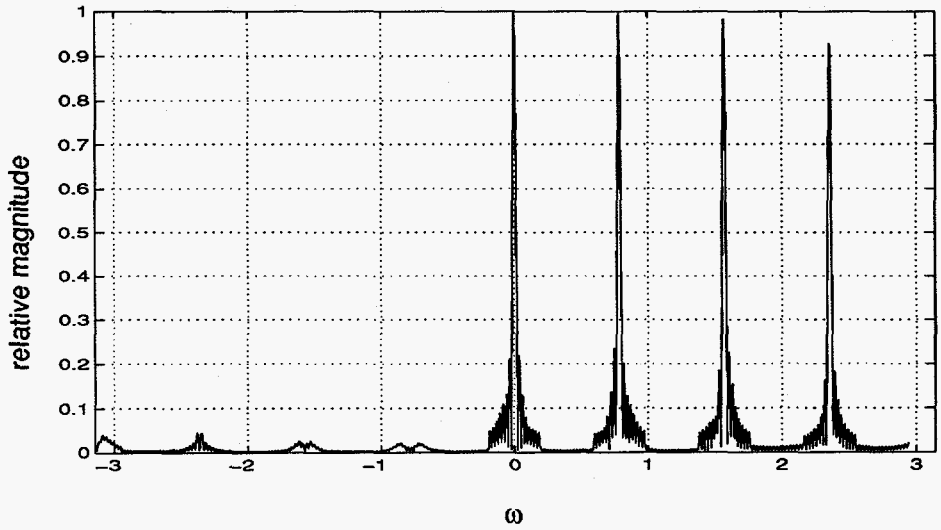

Figure 3. Example processed with one tier of subapertures.

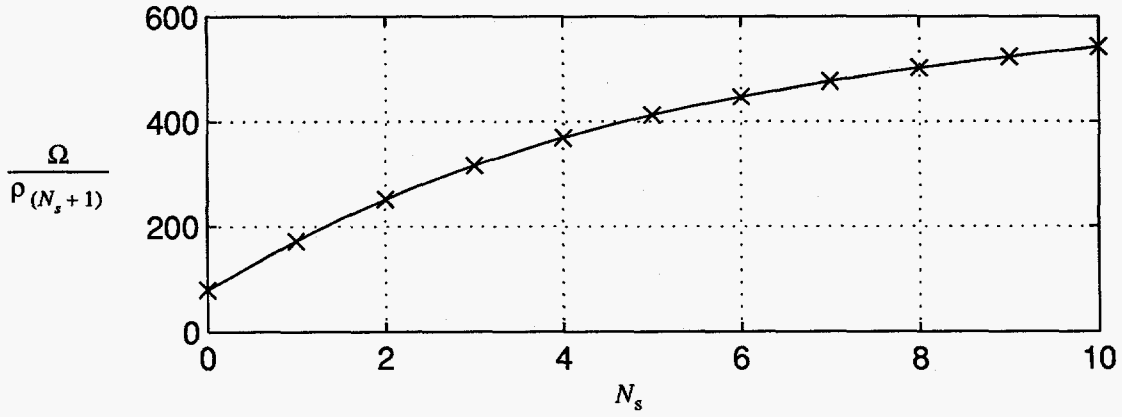

Figure 4. Limits on Ω for a = 0.0001.

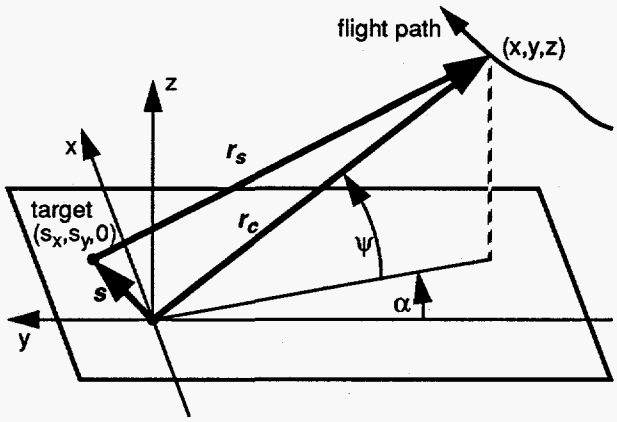

Figure 5. SAR geometry.

$$X_V(i,n) \approx A(r_{s,0}) \ \exp j\left\{\frac{2}{c}[\omega_n + \gamma_n T_s i]\cos\psi_n \cos\alpha_n (s_x \tan\alpha_n - s_y + \xi_r) + \frac{2\gamma_n}{c^2}\cos\psi_n \cos\alpha_n \xi_p\right\}. \tag{12}$$

where $A(r_{s,0})$ represents the amplitude of the echo from the target. The functions ξ_r and ξ_p represent spatially variant error terms that can be described by polynomials in n. By adjusting ω_n and γ_n to compensate for variations in $\cos\psi_n$ and $\cos\alpha_n$, and sampling at equal increments in $\tan\alpha_n$, equation (12) can be simplified to

$$X_V(i,n) = A(r_{s,0}) \ \exp j\left\{\frac{2\omega_0\cos\psi_0}{c}\left(\left[1 + \frac{\gamma_0 T_s}{\omega_0} i\right](s_x d\alpha\ n - s_y + \xi_r) + \frac{\gamma_0}{\omega_0 c}\xi_p\right)\right\}. \tag{13}$$

The processing strategy is then to resample along n as a function of $(1+(\gamma_0 T_s i)/\omega_0)$, followed by a 2-dimensional DFT over i and the resampled n. This can be accomplished by employing a chirp-Z transform (CZT) over n that incorporates the resampling, followed by a FFT over i. Recall that the CZT can be implemented with FFTs and vector multiplies. By limiting the largest quadratic error term in ξ_r to less than $\pi/2$, Walker calculated the size limit for an individual patch approximately to diameters

$$D_x, D_y \le 4\rho_x (\|r_{c0}\|/\lambda_0)^{1/2}, \tag{14}$$

where ρ_x is the nominal resolution in the x-direction at the scene center, $\|r_{c0}\|$ is the nominal range to the scene center, and λ_0 is the nominal wavelength of the radar, $\lambda_0 = 2\pi c/\omega_0$.

By accounting for error ξ_p, a general quadratic phase error limit, elevation angles, and pulse widths, the patch diameter limits can be refined to

$$D_x \le 4\rho_x \sqrt{\frac{\left(2(\cos\psi_0)^2\right)\left(\frac{\phi_n}{\pi/2}\right)\left(\frac{\|r_{c,0}\|}{\lambda_0}\right)}{\left(1 + \frac{\gamma_0 T_{eff}}{2\omega_0} + \frac{4\gamma_0\|r_{c,0}\|(\cos\psi_0)^2}{\omega_0 c}\right)}}, \qquad D_y \le 4\rho_x \sqrt{\frac{\left(\frac{2(\cos\psi_0)^2}{1+(\cos\psi_0)^2}\right)\left(\frac{\phi_n}{\pi/2}\right)\left(\frac{\|r_{c,0}\|}{\lambda_0}\right)}{\left(1 + \frac{\gamma_0 T_{eff}}{2\omega_0} + \frac{2\gamma_0\|r_{c,0}\|(\cos\psi_0)^2}{\omega_0 c\left(1+(\cos\psi_0)^2\right)}\right)}}, \tag{15}$$

where $T_{eff} = T_s I$ is the effective pulse width of the radar.

4. PROCESSING WITH TIERS OF SUBAPERTURES

4.1. One Tier of Subapertures

Now reconsider equation (13) where both indices i and n are each divided into a single tier of subapertures, analogous to equation (4),

$$n = m_1 + \Delta_2 m_2 \text{, and} \quad i = k_1 + \mu_2 k_2 . \tag{16}$$

Equation (13) then becomes

$$X_V(k_1, k_2, m_1, m_2) \approx A(r_{s,0}) \exp j\left\{\frac{2\omega_0 \cos\psi_0}{c}\left(\left[1+\frac{\gamma_0 T_s \mu_2}{\omega_0}k_2 + \frac{\gamma_0 T_s}{\omega_0}k_1\right](s_x\Delta_2 m_2 + s_x m_1 - s_y + \xi_r) + \frac{\gamma_0}{\omega_0 c}\xi_p\right)\right\} . \tag{17}$$

The processing strategy is straightforward and is illustrated in figure 6.

1. perform a CZT across m_1, adjusting output sample spacing as a function of k_1 and k_2. Use the resulting estimate of s_x to compensate the phase of the result.

2. perform a FFT across k_1. Use the result to optimally estimate s_x and s_y to further compensate the phase of the result.

3. perform a CZT across m_2, adjusting output sample spacing as a function of k_2. Use the result to again optimally estimate s_x and s_y to further compensate the phase of the result.

4. perform a FFT across k_2. The result is the complex SAR image.

Note that the error functions ξ_r and ξ_p formerly being polynomials in n, now contains a number of cross product terms between m_1 and m_2. The cross terms that are linear coefficients of the index being transformed manifest themselves as migration terms. Migration has the effect of windowing the data and thereby limiting the resolution of succeeding transforms. It is therefor necessary to limit migration to something on the order of one resolution cell across the entire aperture. This is done by limiting subaperture length, and hence subaperture resolution. Since migration affects succeeding transforms, resolution limits due to migration only affect the stages prior to the final transforms, and tend to dominate the effects of other error terms that broaden the impulse response. The final transform pair, however, are over data that contains no cross-product migration terms (or at least none that can't be accommodated by the final CZT) and therefor have resolutions limited by spatially variant phase errors, specifically the quadratic component of the error function.

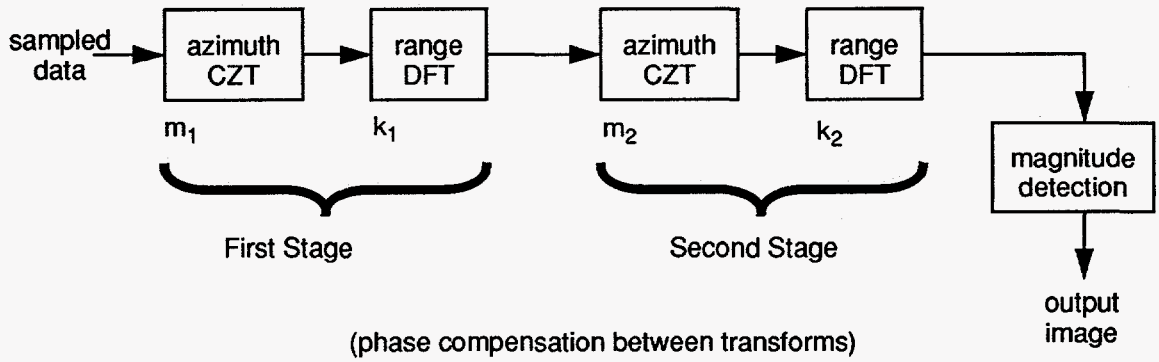

Figure 6. Processing with 1 tier of azimuth subapertures, and1 tier of range subapertures.

The first stage suffers migration, and when migration is limited to σ_{m_1} resolution cells, patch diameters are limited to

$$D_x^2 \le 16\rho_{x,1}\rho_{x,2}\sigma_{m_1}(\cos\psi_0)^2\left(\frac{\|\boldsymbol{r}_{c,0}\|}{\lambda_0}\right)\left(1-\frac{\gamma_0 T_{eff}}{2\omega_0}\right)\left(1-\frac{\gamma_0 T_{eff}}{2\omega_0}+\frac{4\gamma_0\|\boldsymbol{r}_{c,0}\|(\cos\psi_0)^2}{\omega_0 c}\right)^{-1}, \text{ and} \tag{18}$$

$$D_y^2 \le 16\rho_{x,1}\rho_{x,2}\sigma_{m_1}\left(\frac{(\cos\psi_0)^2}{1+(\cos\psi_0)^2}\right)\left(\frac{\|\boldsymbol{r}_{c,0}\|}{\lambda_0}\right)\left(1-\frac{\gamma_0 T_{eff}}{2\omega_0}\right)\left(1-\frac{\gamma_0 T_{eff}}{2\omega_0}+\frac{2\gamma_0\|\boldsymbol{r}_{c,0}\|(\cos\psi_0)^2}{\omega_0 c\left(1+(\cos\psi_0)^2\right)}\right)^{-1}. \tag{19}$$

where D_x and D_y are the scene diameters in the x and y directions respectively, $\rho_{x,1}$ and $\rho_{y,1}$ are the resolutions in the x and y directions after the first CZT / FFT transform pair, and $\rho_{x,2}$ and $\rho_{y,2}$ are the resolutions in the x and y directions after the second and final CZT / FFT transform pair. We also define $\delta_{x,1}$ and $\delta_{x,2}$ as the first stage's pixel spacing in the x and y directions respectively.

Limiting the quadratic component of the spatially variant phase errors to about ϕ_{m_2} limits the final stage CZT / FFT transform pair such that

$$\delta_{x,1}D_x \le 8\left(\frac{\rho_{x,2}}{a_{w,m_2}}\right)^2(\cos\psi_0)^2\left(\frac{\phi_{m_2}}{\pi/2}\right)\left(\frac{\|\boldsymbol{r}_{c,0}\|}{\lambda_0}\right)\left(1+\frac{\gamma_0 T_{eff}}{2\omega_0}+\frac{4\gamma_0\|\boldsymbol{r}_{c,0}\|(\cos\psi_0)^2}{\omega_0 c}\right)^{-1}, \text{ and} \tag{20}$$

$$\delta_{y,1}D_y \le 8\left(\frac{\rho_{x,2}}{a_{w,m_2}}\right)^2\left(\frac{(\cos\psi_0)^2}{1+(\cos\psi_0)^2}\right)\left(\frac{\phi_{m_2}}{\pi/2}\right)\left(\frac{\|\boldsymbol{r}_{c,0}\|}{\lambda_0}\right)\left(1+\frac{\gamma_0 T_{eff}}{2\omega_0}+\frac{2\gamma_0\|\boldsymbol{r}_{c,0}\|(\cos\psi_0)^2}{\omega_0 c\left(1+(\cos\psi_0)^2\right)}\right)^{-1}. \tag{21}$$

Assuming that $\rho_{y,1} \approx \rho_{x,1}$ allows us to calculate overall limits by combining equations (18) thru (21) to yield

$$D_x \le 4\rho_{x,2}\left(\frac{2(\cos\psi_0)^4\left(a_{os,m_1}\sigma_{m_1}\right)\left(\frac{\phi_{m_2}}{\pi/2}\right)\left(\frac{\|\boldsymbol{r}_{c,0}\|}{\lambda_0}\right)^2\left(1-\frac{\gamma_0 T_{eff}}{2\omega_0}\right)}{\left(1-\frac{\gamma_0 T_{eff}}{2\omega_0}+\frac{4\gamma_0\|\boldsymbol{r}_{c,0}\|(\cos\psi_0)^2}{\omega_0 c}\right)\left(1+\frac{\gamma_0 T_{eff}}{2\omega_0}+\frac{4\gamma_0\|\boldsymbol{r}_{c,0}\|(\cos\psi_0)^2}{\omega_0 c}\right)}\right)^{\frac{1}{3}}, \text{ and} \tag{22}$$

$$D_y \le 4\left(\frac{\rho_{x,2}}{a_{w,m_2}}\right)\left(\frac{2\left(\frac{(\cos\psi_0)^2}{1+(\cos\psi_0)^2}\right)^2\left(a_{os,k_1}\sigma_{m_1}\right)\left(\frac{\phi_{m_2}}{\pi/2}\right)\left(\frac{\|\boldsymbol{r}_{c,0}\|}{\lambda_0}\right)^2\left(1-\frac{\gamma_0 T_{eff}}{2\omega_0}\right)}{\left(1-\frac{\gamma_0 T_{eff}}{2\omega_0}+\frac{2\gamma_0\|\boldsymbol{r}_{c,0}\|(\cos\psi_0)^2}{\omega_0 c\left(1+(\cos\psi_0)^2\right)}\right)\left(1+\frac{\gamma_0 T_{eff}}{2\omega_0}+\frac{2\gamma_0\|\boldsymbol{r}_{c,0}\|(\cos\psi_0)^2}{\omega_0 c\left(1+(\cos\psi_0)^2\right)}\right)}\right)^{\frac{1}{3}}. \tag{23}$$

which is an improvement over the limits given in equations (15).

4.2. Multiple Tiers of Subapertures

Note that the initial sampling strategy along with the CZT make each stage a separate polar-format processed image formation step, but allows successive stages to achieve finer resolution. This strategy can be extended in a similar manner to an arbitrary number of tiers of subapertures. Any number N_s tiers will require N_s+1 stages of FFT / CZT pairs, partitioned with indices

$$n = m_1 + \sum_{p=2}^{N_s+1} \left[m_p \prod_{q=2}^{p} \Delta_q \right], \text{ and} \qquad i = k_1 + \sum_{p=2}^{N_s+1} \left[k_p \prod_{q=2}^{p} \mu_q \right]. \tag{24}$$

The architecture for such a scheme is illustrated in figure 7. Overall limits on patch diameters can then be extended to

$$D_x \le 4\rho_{x,\,(N_s+1)} \left(\frac{\left(2\left(a_{os,m_1} \ldots a_{os,m_{N_s}} \right)\left(\sigma_{m_1} \ldots \sigma_{m_{N_s}} \right)\left(\frac{\phi_{m_{(N_s+1)}}}{\pi/2} \right) \times (\cos\psi_0)^{2(N_s+1)} \left(\frac{\|\boldsymbol{r}_{c,0}\|}{\lambda_0} \right)^{(N_s+1)} \left(1 - \frac{\gamma_0 T_{eff}}{2\omega_0} \right)^{N_s} \right)^{\frac{1}{(N_s+2)}}}{\left(1 - \frac{\gamma_0 T_{eff}}{2\omega_0} + \frac{4\gamma_0 \|\boldsymbol{r}_{c,0}\| (\cos\psi_0)^2}{\omega_0 c} \right)^{N_s} \left(1 + \frac{\gamma_0 T_{eff}}{2\omega_0} + \frac{4\gamma_0 \|\boldsymbol{r}_{c,0}\| (\cos\psi_0)^2}{\omega_0 c} \right)} \right), \text{ and} \tag{25}$$

$$D_y \le 4\rho_{x,\,(N_s+1)} \left(\frac{\left(2\left(a_{os,k_1} \ldots a_{os,k_{N_s}} \right)\left(\sigma_{m_1} \ldots \sigma_{m_{N_s}} \right)\left(\frac{\phi_{m_{(N_s+1)}}}{\pi/2} \right) \times \left(\frac{(\cos\psi_0)^2}{1 + (\cos\psi_0)^2} \right)^{(N_s+1)} \left(\frac{\|\boldsymbol{r}_{c,0}\|}{\lambda_0} \right)^{(N_s+1)} \left(1 - \frac{\gamma_0 T_{eff}}{2\omega_0} \right)^{N_s} \right)^{\frac{1}{(N_s+2)}}}{\left(1 - \frac{\gamma_0 T_{eff}}{2\omega_0} + \frac{2\gamma_0 \|\boldsymbol{r}_{c,0}\| (\cos\psi_0)^2}{\omega_0 c\left(1 + (\cos\psi_0)^2 \right)} \right)^{N_s} \left(1 + \frac{\gamma_0 T_{eff}}{2\omega_0} + \frac{2\gamma_0 \|\boldsymbol{r}_{c,0}\| (\cos\psi_0)^2}{\omega_0 c\left(1 + (\cos\psi_0)^2 \right)} \right)} \right). \tag{26}$$

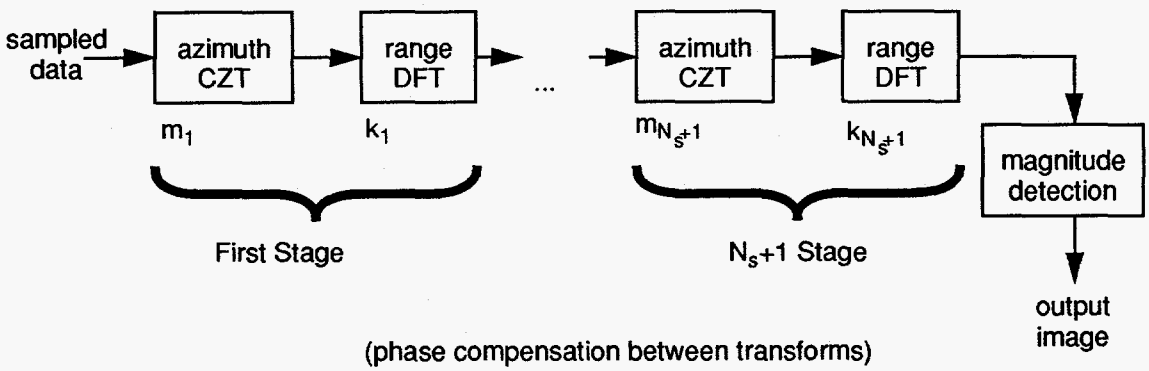

Figure 7. Processing with N_s tiers of azimuth subapertures, and N_s tiers of range subapertures.

For scene diameters less than this limit, and particularly when image aspect ratios are non-unity, $D_x \neq D_y$, the assumption that each stage's output resolutions be equal in the x and y directions, $\rho_{y,n_s} = \rho_{x,n_s}$, may be relaxed, even to the point that a particular transform in some stage collapses to unity length, that is, vanishes. In any case, the relationship between intermediate resolutions need to be chosen to comply with the migration limitations, whereas the relationship between final resolutions need to concern themselves with spatially variant phase error limitations.

5. EXAMPLES - LIMITS AND IMAGES

Equations (25) and (26) can be parametrically plotted. Figure 8 does so for a UHF SAR with nominal center frequency at 300 MHz.

Sandia National Laboratories currently operates a SAR capable of collecting data in the UHF region of the spectrum. The SAR flies on a DeHavilland DH-6 (Series 300) "Twin Otter" aircraft. Figure 9 illustrates an image of a 2 km wide view of Estancia, NM, collected from a 4.6 km range with a 380 MHz center frequency and processed to 2 m resolution with polar format processing. Figure 10 illustrates the same data processed with one tier of subapertures in both range and azimuth. The subapertures allow focussing even in the lower corners of the view.

6. DISCUSSION

Employing subapertures increases the number of dimensions of the phase history model (initial data set). While seemingly more complicated, as each dimension is in turn processed, this strategy allows a gradual shift from the data domain to the image domain. In the process, we are at times partly in each domain, which allows us coarse resolution estimates of target positions as well as coarse resolution estimates of the SAR's aperture position. This in turn allows us to compensate phase errors that are functions of cross-coupled parameters from both domains, that is, spatially variant phase errors. This is why subapertures work. The limits on subaperture processing are due to migration terms in the coarse resolution position estimates. Controlling these requires limiting the stage-to-stage resolution enhancement. Therefore, patch diameter limits still do exist

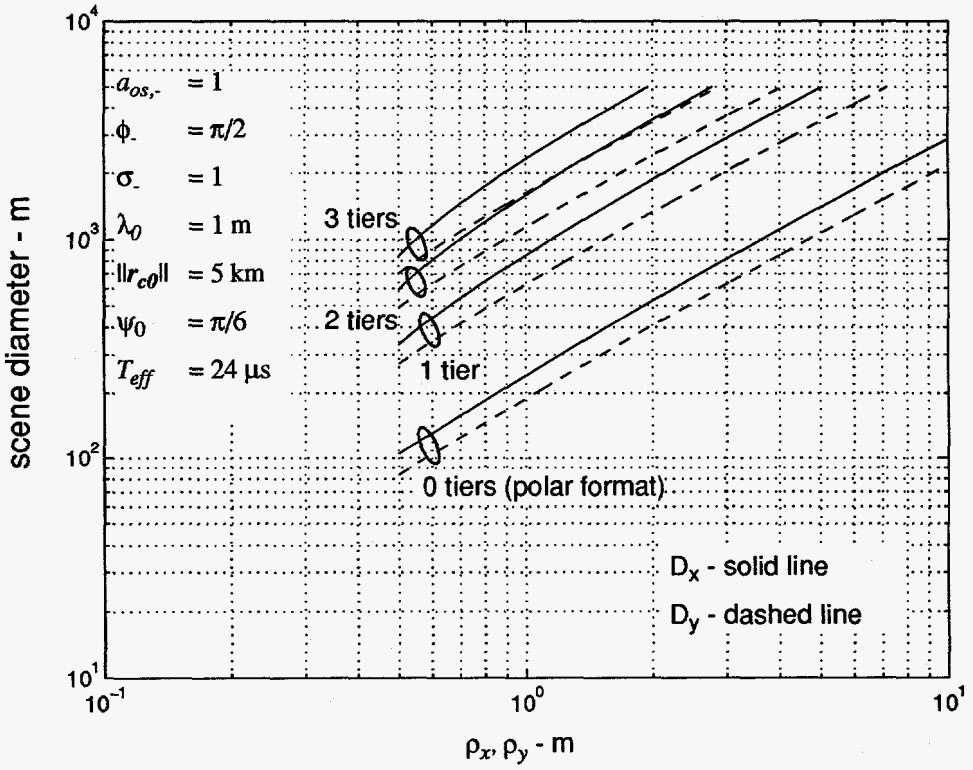

Figure 8. UHF-band SAR (300 MHz).

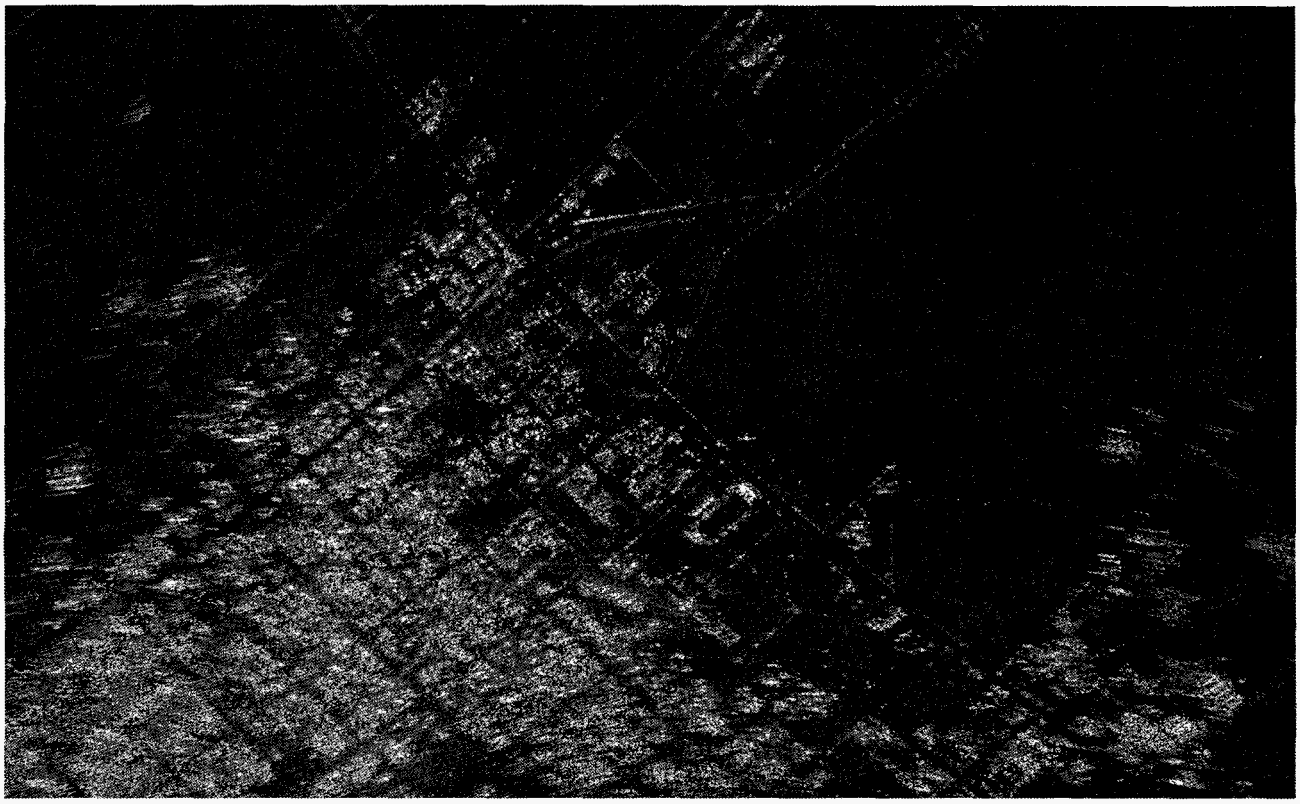

Figure 9. UHF image of Estancia, NM, processed to 2 m resolution with no subapertures.

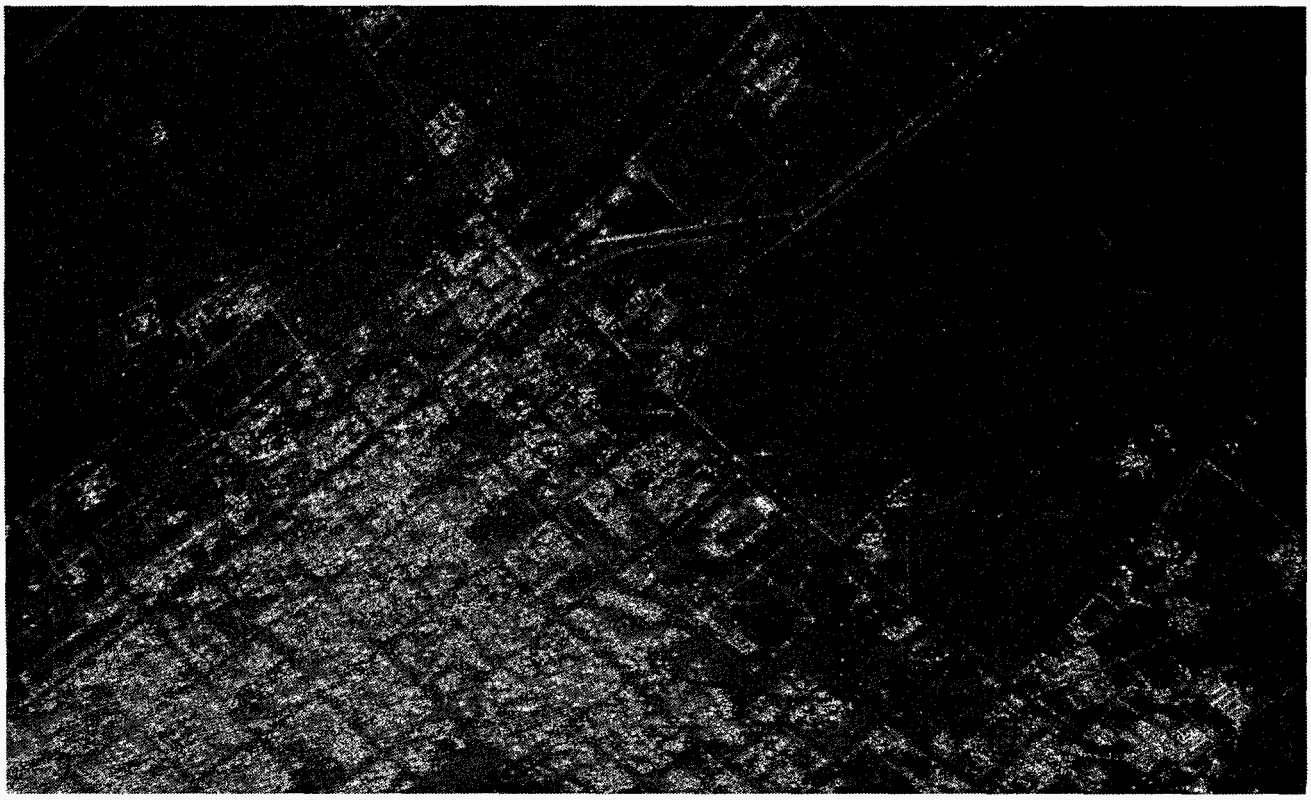

Figure 10. UHF image of Estancia, NM, processed to 2 m resolution with one tier of subapertures.

for subaperture processing. These limits can, however, be extended by employing yet more tiers of subapertures. Each additional tier of subapertures enhances the achievable patch diameter, but with diminishing returns. The first tier offers the most relative improvement, and the second tier offers more relative improvement than the third tier, etc. Generally, azimuth patch diameters exceed range patch diameters, but this is true for polar format processing as well. Oversampling the coarse resolution outputs allows further improvement, although in the extreme this causes a degeneration of the algorithm to matched filtering.

Tiered subapertures are most useful when image resolutions are desired to approach the wavelength of the SAR. This is no more desirable than with SARs operating in the UHF region of the spectrum, or lower. Traditional image formation algorithms might offer patch diameters of only a few hundred meters, whereas employing subapertures might push the limit to several kilometers. Wide angle images from Sandia Laboratories UHF SAR have been successfully formed using range and azimuth subapertures.

7. ACKNOWLEDGMENTS

This work performed at Sandia National Laboratories is supported by the U.S. Department of Energy under contract DE-AC04-94AL85000.

8. REFERENCES

1. Ausherman, Dale A., Adam Kozma, Jack L. Walker, Harrison M. Jones, Enrico C. Poggio, "Developments in Radar Imaging", IEEE Transactions on Aerospace and Electronic Systems, Vol. AES-20, No. 4, pp 363-398, July 1984.

2. Burns, B. L., J. T. Cordaro, "SAR image formation algorithm that compensates for the spatially variant effects of antenna motion", SPIE Proceedings, Vol 2230, SPIE's International Symposium on Optical Engineering in Aerospace Sensing, Orlando, 4-8 April 1994.

3. Caputi, William J. Jr., "Stretch: A Time-Transformation Technique", IEEE Transactions on Aerospace and Electronic Systems, Vol. AES-7, No. 2, pp 269-278, March 1971.

4. Doerry, A. W., "Synthetic Aperture Radar Processing with Polar Formatted Subapertures", Proceedings of the 28th ASILOMAR Conference, Pacific Grove, California, Oct. 31 - Nov. 2, 1994.

5. Doerry, A. W., Synthetic Aperture Radar Processing with Tiered Subapertures, Ph.D. Dissertation, University of New Mexico, May, 1995.

6. Flynn, Thomas J., "Wavenumber-Domain SAR Focusing from a Nonuniform Synthetic Aperture", Proceedings of the IEEE 1992 International Conference on Acoustics, Speech, and Signal Processing (ICASSP-92), March 1992.

7. Lawton, Wayne, "A New Polar Fourier Transform for Computer-Aided Tomography and Spotlight Synthetic Aperture Radar", IEEE Transactions on Acoustics, Speech, and Signal Processing, Vol. 36, No. 6, pp 931-933, June 1988.

8. Perry, R. P., R. C. DiPietro, A. Kozma, J.J. Vaccaro, "SAR Image formation processing using planar subarrays", SPIE Proceedings, Vol 2230, SPIE's International Symposium on Optical Engineering in Aerospace Sensing, Orlando, 4-8 April 1994.

9. Walker, Jack L., "Range-Doppler Imaging of Rotating Objects", IEEE Transactions on Aerospace and Electronic Systems, Vol. AES-16, No. 1, pp 23-51, January 1980.

10. Oppenheim, Alan V., Ronald W. Schafer, Digital Signal Processing, Prentice-Hall, Inc., Englewood Cliffs, New Jersey, 1975, ISBN 0-13-214635-5.